J Mol Model (2009) 15:433–446
DOI 10.1007/s00894-008-0385-x

ORIGINAL PAPER

The zinc complex catalyzed hydration of alkyl isothiocyanates

Wilhelm A. Eger · Burkhard O. Jahn · Ernst Anders

Received: 2 September 2008 / Accepted: 9 October 2008 / Published online: 16 December 2008

Abstract Based upon our preceding studies of the hydration of CO_2, COS and CS_2, accelerated by the carbonic anhydrase (CA) using simplified $[ZnL_3OH]^+$ complexes as model catalysts, we calculated the hydration mechanisms of both the uncatalyzed and the $[ZnL_3OH]^+$-catalyzed reactions (L=NH_3) of isothiocyanates RNCS on the B3LYP/6-311+G(d,p) level of theory. Interestingly, the transition state for the favored metal mediated reaction with the lowest Gibbs free energy is only slightly higher than in the case of CO_2 (depending on the attacking atom (N or S). Calculations under inclusion of solvent corrections show a reduction of the selectivity and a slight decrease of the Gibbs free energy in the rate-determining steps. The most plausible pathway prefers the mechanism via a Lindskog proton-shift transition state leading to the thermodynamically most stable product, the carbamatic-S-acid. Furthermore, powerful electron withdrawing substituents R of the cumulenic substrates influence the selectivity of the reaction to a significant extent. Especially the CF_3-group in trifluoromethylisothiocyanate reverses the selectivity. This investigation demonstrates that reaction principles developed by nature can be translated to develop efficient catalytic methods, in this case presumably for the transformation of a wide variety of heterocumulenes aside from CO_2, COS and CS_2.

Keywords Carbonic anhydrase · Density functional calculations · Enzyme models · Isothiocyanate fixation

Introduction

The enzyme carbonic anhydrase (CA) is a ubiquitous enzyme with a Zn^{2+} ion as a cofactor and is essential for many living organisms. It catalyzes the hydration of CO_2 and accelerates this reversible reaction by a factor of 10^7 in comparison to the uncatalyzed reaction [1–5].

Human carbonic anhydrase II (HCAII), the fastest of the known isoenzymes, has a turnover number of $10^6 s^{-1}$ at 25 °C and pH 9 [6–8]. Because of the reversibility of this reaction, the pH value plays an important role. At pH 7 to 9 the hydration of CO_2 takes place, whereas at pH values below 7, dehydration is preferred. The active site of the HCAII consists of a Zn^{2+} ion and three histidine residues (His94, His96, His119). The Zn^{2+} ion has a tetrahedral coordination sphere. The fourth ligand is a water molecule, which is linked to the solvent by a proton network. Obviously, in the natural catalytic cycle a fourth histidine residue (His64) near to the active site plays an important role, especially for the reversible protonation/deprotonation steps [9]. Several theoretical investigations at different theoretical levels with different models for HCAII exist [10–13]. We recently investigated the reaction mechanism of the natural substrates CO_2 and COS by application of density functional theory (DFT) calculations [14–17].

We have shown that the most simple model $[Zn(NH_3)_3OH]^+$ can be used to simulate the active site of HCAII. This complex does not exist in solution under ambient conditions but in a high vacuum it survives as a stable gas-phase species and allows the investigation of important reaction steps [18]. Therefore it might be a good

Electronic supplementary material The online version of this article (doi:10.1007/s00894-008-0385-x) contains supplementary material, which is available to authorized users.

W. A. Eger · B. O. Jahn · E. Anders (✉)
Institute of Organic Chemistry and Macromolecular Chemistry,
Friedrich Schiller University Jena,
Humboldtstrasse 10,
07743 Jena, Germany
e-mail: Ernst.Anders@uni-jena.de

starting point to estimate the possibility of assigning the principle of catalysis to model complexes in synthesis.

As depicted in Scheme 1, the reaction path starts with an encounter complex (EC) **CO_2_1** of CO_2 and the CA model. Via the transition structure **CO_2_2(ts)**, which characterizes the rate-determining step, it proceeds to the first intermediate **CO_2_3** [19]. For the consecutive steps, the DFT calculations demonstrate the slight preference of the so called "Lindskog" transition state **CO_2_4(ts)**, which describes the rotation around the bond between the carbon and the zinc coordinated oxygen atom. The alternative "Lipscomb" transition state represents a proton shift from the hydroxyl group to the double-bonded oxygen to give **CO_2_5** which could be catalyzed by water [20, 21]. In the final step carbonic acid is released after a water attack (**CO_2_8**). Thereby the catalytic cycle is closed as the catalyst $[Zn(NH_3)_3OH]^+$ is regenerated. Although it is well known that an alternative mechanism exists, these reaction steps seem to be the only possibilities for an application on model complexes in experiment because they are missing the protein backbone of HCAII.

Our goal is the extension of this natural "mode of action" to a wide variety of heterocumulene substrates similar to CO_2 in order to develop novel catalytic reaction paths with simple complexes which emulate the catalytic center of HCAII. In this work we will discuss whether the reaction of isothiocyanates (**ITCN**) with water and further related substrates can be catalyzed by such a catalytically active complex. In order to allow calculations on a sufficient level of theory, we again used the model complex $[Zn(NH_3)_3OH]^+$.

Ionized isothiocyanate is a well known inhibitor for HCAII [22]. It reacts by displacing the zinc bound hydroxide. There are even experimental studies of reactions with HCAII emulating models [23]. As we use neutral methylisothiocyanate and respectively other substituted

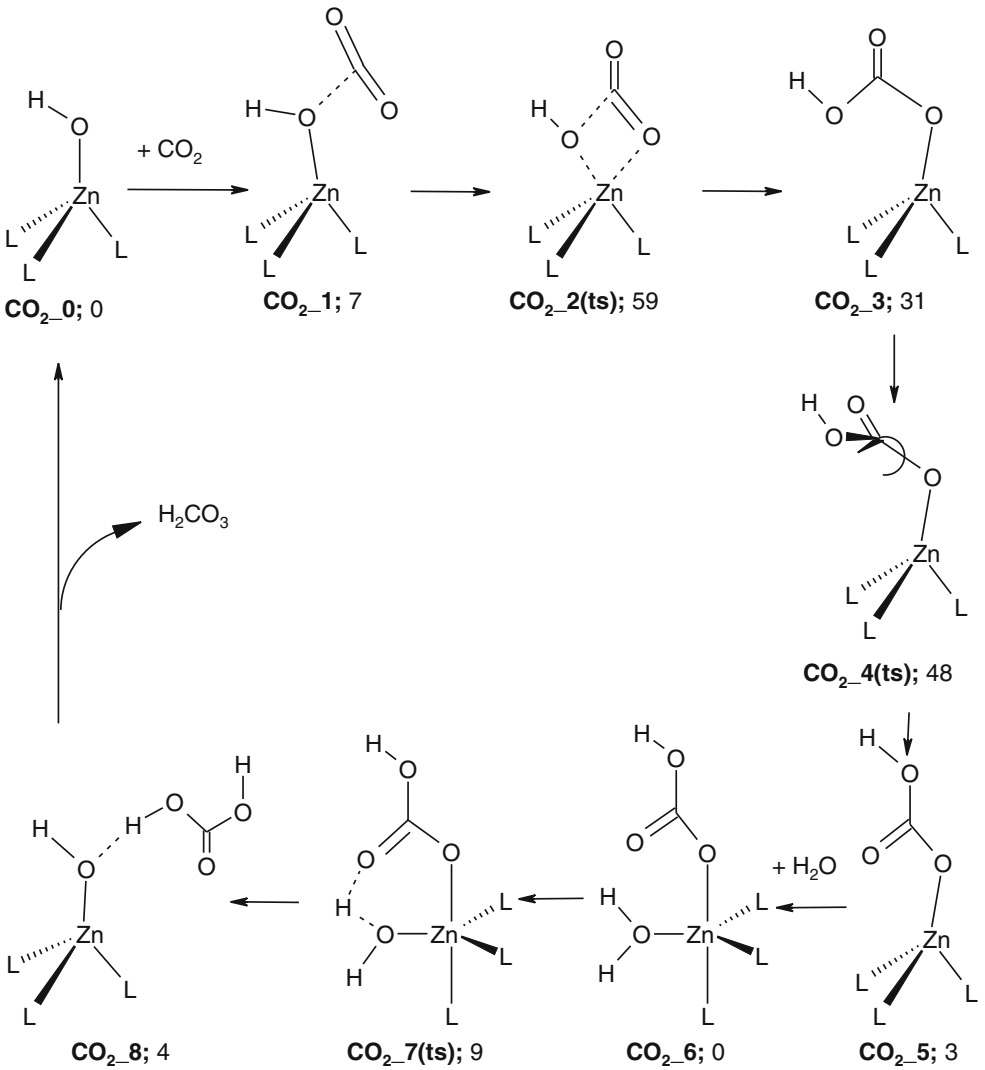

Scheme 1 The catalytic cycle of $[Zn(NH_3)_3OH]^+$ and CO_2. Gibbs free energies in kJ/mol. These structures were recalculated using *Gaussian03* and are based on the results of S. Schenk et al. [14] Schenk S, Kesselmeier J, Anders E (2004) Chem Eur J 10:3091–3105

isothiocyanates, our substrate presumably will not react as an inhibitor but will follow a pathway comparable with that of CO_2.

Computational methods

The hybrid density functional B3LYP [24, 25] with the 6-311+G(d,p) basis set [26, 27] was used for the catalyzed reaction. The uncatalyzed reaction was additionally calculated at the MP2 [28, 29] level using a AUG-cc-pVTZ [30, 31] basis due to the smaller system. Previous investigations have demonstrated reliable results on this level of theory for systems like $[Zn(NH_3)_3OH]^+$ [14, 15]. Full geometry optimizations, i.e., without constraints, as well as frequency calculations on the stationary points thus obtained were performed for all species on the hyper surface in the gas-phase as well as in the presence of a dielectric field as described by the C-PCM model for selected structures [32–34]. In this model, the species of interest are embedded in a cavity of molecular shape surrounded by a polarizable continuum whose field modifies the energy and physical properties of the solute. The solvent reaction field is described by polarization charges distributed on the cavity surface. This procedure is known to reproduce experimental solvation energies quite well. We chose several solvents with different dielectric field constants from $\varepsilon=0$ (gas phase) up to $\varepsilon=78.39$ for water (heptane, chloroform, dichloroethane, acetonitrile and water).

All optimizations and frequency calculations reported in this article were performed using the *Gaussian03* program package [35]. Atomic charges and hyperconjugative interaction energies were obtained using version 5.1 of the natural bond orbital (NBO) analysis of Weinhold et al. [36–39]. Default convergence criteria were used for all calculations. All energies reported are unscaled Gibb's free energies (ΔG values) and thus contain zero-point, thermal and entropy effects at 298K and 1 atmosphere pressure.

Results and discussion

Uncatalyzed reactions

In order to define an energetic standard, we started with the investigation of the uncatalyzed hydration of isothiocyanates (**ITCN**) and continued with their $[ZnL_3\text{-}OH]^+$ catalyzed counterparts.

The uncatalyzed reaction of isothiocyanates with water is obviously extremely slow [40] and further, this reaction is poorly described in the literature. Methylisothiocyanate is not soluble in and consequently does not react with water. Alcohols must be heated up to 10–20 hours with isothiocyanates to react quantitatively [41]. Only nitrophenylisothiocyanates can react rapidly in boiling ethanol [42]. The reaction with methanol is also very slow [43]. Kinetic investigations of the reaction of isothiocyanates with alcohols were performed in presence of a catalyst, e. g., triethylamine [41, 44]. To gain insight into the mechanism and especially information concerning the energetic background, we started the DFT investigation of the uncatalyzed addition of water to methylisothiocyanate **U_1** (all species for this section are depicted in Scheme 2), which should serve as a standard and allows comparison with the metal-catalyzed reaction.

At first, all possible tautomers of all possible products were calculated and the thermodynamically most stable species was determined (**U_5**). The relative stability of this species results mostly from the preferred C=O double bond as estimated by Hadad et al. [45]. Obviously, there is also a slight negative hyperconjugational effect as the C-N bond in **U_5** is about 0.022 Å longer than in **U_3** [46]. To model isothiocyanates (**ITCN**) we used the simplest example, methylisothiocyanate. All Gibbs free energies given in conjunction with the uncatalyzed reaction of **ITCN** and water refer to the sum of the Gibbs free energies of the separated reactants (methylisothiocyanate and water, **U_0**).

There are two transition states that could be the rate-determining step (**U_2a(ts)** and **U_2(ts)**). The first one represents the addition of water to the N=C double bond. The second is the same reaction catalyzed by an additional water molecule which serves as a proton shuttle (cf. Scheme 2). The transition states differ remarkably in their Gibb's enthalpies. **U_2(ts)** (158 kJ/mol) is ca. 48 kJ/mol more stable than **U_2a(ts)** (206 kJ/mol). This results from the six-membered cyclic transition state, which is energetically more favorable than the four-membered cyclic transition state. After surmounting the rate-determining step under formation of **U_3**, the most stable product **U_5** is formed via **U_4(ts)**. As a consequence of these calculations this path to **U_5** can be understood to be the most favored one. None of the subsequent transition states have a higher energy than the rate-determining step **U_2(ts)**.

The addition of water molecule to the C=S double bond is not preferred, as both the transition states and the following intermediates possess significantly higher Gibbs free energies than in case of the N=C double bond hydration (cf. Supporting Information).

As carbamatic-S-acid decomposes to give COS and methylamine, we also calculated the mechanism for that reaction. The rate determining step of the decomposition mechanism is about 54 kJ/mol lower than **U_2(ts)**. COS and methylamine as separated products are about −31 kJ/mol stabilized compared to the separated reactants methylisothiocyanate and water. Further details of this reaction step are assembled in the Supporting Information.

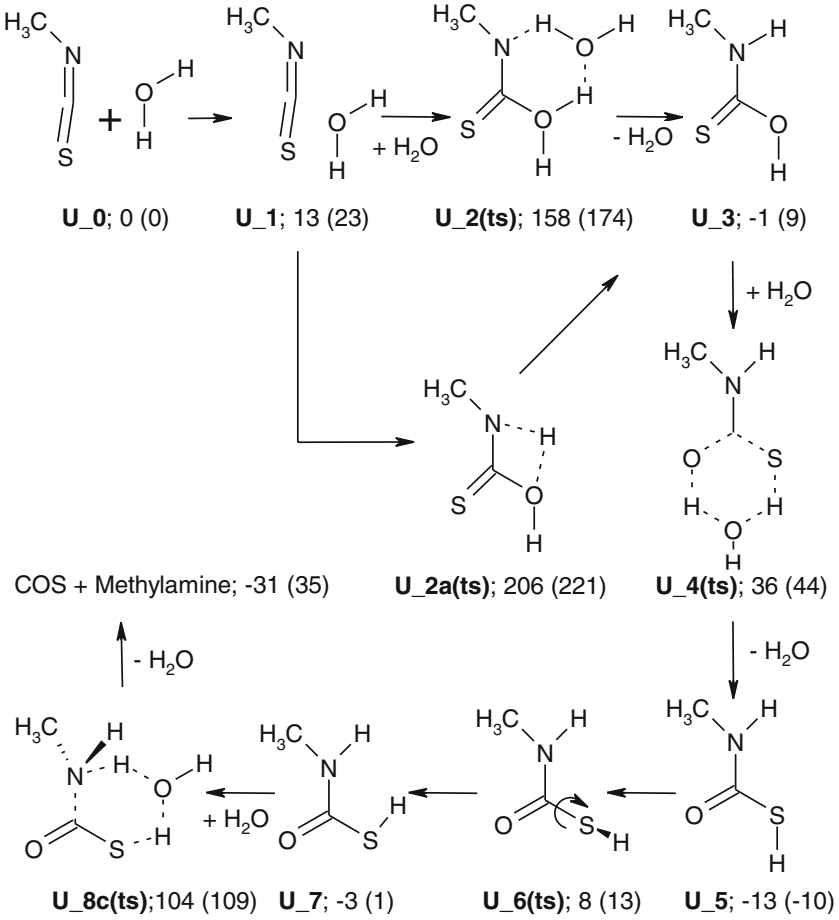

Scheme 2 The most convenient mechanism of the uncatalyzed reaction of **ITCN** and water. Gibbs free energies in kJ/mol are relative to the free products **ITCN** and water. These values are taken from the MP2 level calculations. The values in brackets result from the DFT calculations. A table of free enthalpies and further details of the decomposition of **U_5** can be found in the Supporting Information

Catalytic models

There are many useful models for simulating the active center of the human carbonic anhydrase II; [48] three of them are depicted in Fig. 1. Essential properties are a zinc cation that is coordinated by a hydroxide anion and three ligands coordinating via a nitrogen atom.

The simplest molecule would be the $[Zn(NH_3)_3OH]^+$ complex (Model **I**). The tetrahedral ligand sphere is perturbed by the different symmetry of the hydroxide ion. A hydrogen of one ammonia ligand interacts only slightly with the lone pair of the hydroxide ion. The result of this interaction is a smaller angle between these ligands and a longer bond distance between the involved ammonia ligand

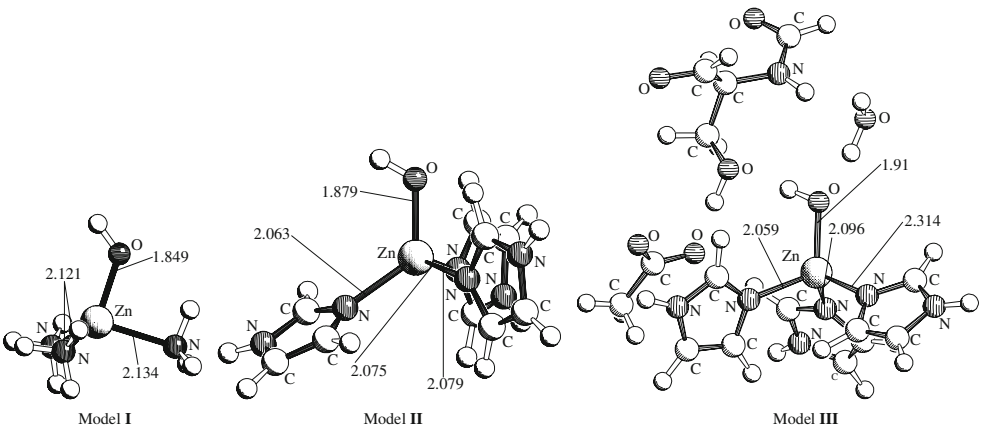

Fig. 1 Three models for simulating the active center of HCAII: Model **I** depicts the $[Zn(NH_3)_3OH]^+$ and Model **II**, the same complex with imidazole ligands. Model **III** was introduced by Bottoni et al. [47]

and the zinc ion. The hydrogen of the hydroxide ion sticks out between two ammonia ligands.

In Model **II** three imidazole residues replace the ammonia ligands. These residues seem to define the sterical situation better than Model **I**, though they break the tetrahedral symmetry slightly more than the ammonia ligands. This results from the steric demand of the imidazole ligands. All N-Zn bonds as well as all angles differ from each other. Yet, due to missing interactions with the lone pair of the hydroxide ion, this model has the lowest differences in N-Zn bond lengths. The hydrogen of the hydroxide ion sticks out over one imidazole ligand, whose tilt decreases the symmetry.

Model **III**, introduced by Bottoni et al. [47], was applied to examine the reaction path of the natural catalytic cycle in HCAII. Bottoni et al. removed most of the backbone of HCAII based on the results of a crystal structure of HCAII under inclusion of a few structures near to the active center and optimized only the inner sphere of his model.

While the O-H bond forms an ecliptic geometry to the Zn-N-bonds in Model **II**, it receives a staggered arrangement in the other two models. The difference in geometry between Model **I** and Model **III** is the missing interaction between the lone pair of the hydroxide ion and the other ligands and the resulting perturbed tetrahedral geometry in Model **I**.

Two factors affect the decision of which model is to be used for the simulation. The first is computing time. Secondly, the model must reliably mimic the properties of a real model complex which can be used in experimental applications. To examine the best approach to the properties of the HCAII center, we performed an NBO calculation [36] on these three models and compared the zinc-oxygen bond lengths and the charge allocation between the two atoms. The calculated values are shown in Table 1.

Little charge variation was found for both oxygen and zinc atoms. A bond length increase results from Model **I** to Model **III**, but the differences are not relevant. Therefore, Model **I** is assumed to sufficiently simulate essential properties of active center of HCAII. Bottoni et al. found a different charge allocation on the models since they used the Mulliken population analysis method, [47, 49] which has been criticized by Guerra et al. [50]. In fact this method depends strongly on the basis set and therefore the Mulliken calculations are not contradictory to the NBO results and to the choice of the catalytically active model, respectively. Anyway, the properties of Model **I** should describe the situation in a model complex sufficiently. Another argument pro Model **I** are the ammonia ligands which presumably build hydrogen bridging bonds to other ligands. As our goal is to assign the catalytic principle to complexes containing ligands like [12]aneN$_3$ or [12]aneN$_4$, those hydrogen bridging bonds bear relation to real systems without the surrounding polypeptide chain.

Table 1 Charges and lengths of the Zn-O bond in the HCAII models

Model	Zn	O	Bond length [Å]
I	+1.62	−1.32	1.849
II	+1.65	−1.31	1.879
III	+1.63	−1.32	1.910

Inhibiton with isothiocyanate

Our intention is the development of a synthetic procedure analogously to the HCAII/CO_2 catalytic cycle which allows the mild and efficient transformation of heterocumulenes such as isothiocyanates. To start this project, we needed DFT based information about details of the well known inhibitor reaction of thiocyanic acid and its anion, respectively [51]. This reaction is depicted in Scheme 3. The first step is the protonation of the hydroxyl group. This step would be catalyzed by His64 of the enzyme. In case of a model without any polypeptide backbone, the direct proton shift is the reasonable mechanism to achieve an aqua

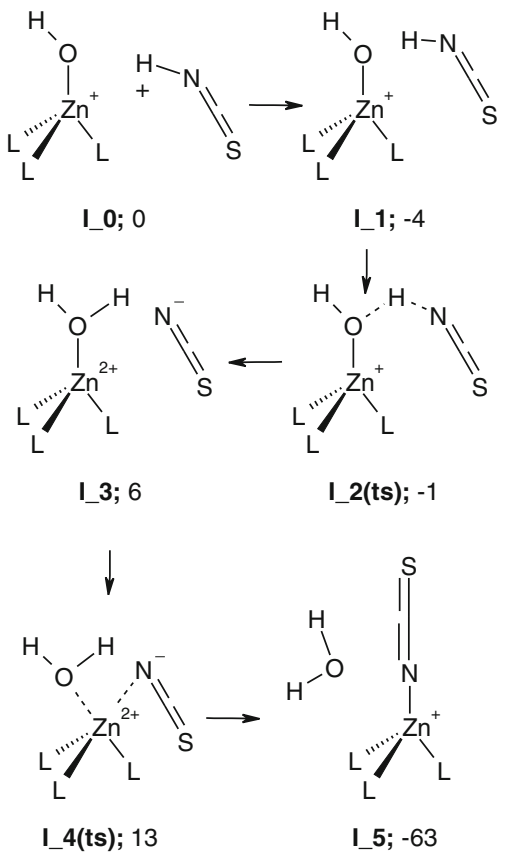

Scheme 3 The inhibition mechanism of isothiocyanate

complex. As the limit of accuracy of the level of theory is about 5 kJ/mol especially in the case of calculating transition states, the relative values of **I_2(ts)** and **I_3** appear to be a little problematic but illustrate impressively the low activation barrier for this transformation.

The protonation step is followed by a ligand exchange via **I_4(ts)** which affords just 13 kJ/mol relative to the separated reactants, a very low activation barrier, too, and is thermodynamically favored by the subsequent formation of the encounter complex **I_5**. This calculation indicates that the reaction of a HCAII model with thiocyanic acid will consequently end under formation of structures such as **I_5** which are relatively stable. Obviously there is no possibility for them to participate in further transformation reactions; their only chance is the back reaction to the free reactants. Preventing the reactants to disappear in such an energetic sink, the proton must be substituted by an alkyl (or aryl) group to increase the feasibility of catalytic reaction cycles similar to HCAII/CO_2 model.

Catalyzed reaction

The reaction pathway is depicted in Schemes 4 and 5, whereas the calculated geometries of the most important intermediates and transition states can be found in Figs. 2, 3, and 4. The full reaction scope can be found in the Supporting Information.

Our investigation indicates that the reaction of **ITCN** with water catalyzed by $[Zn(NH_3)_3OH]^+$ proceeds quite similar compared with the calculated cycle for CO_2 hydration. The catalytic cycle starts with the formation of an EC of methyl **ITCN** with the model catalyst. Several initial arrangements of **ITCN** and $[Zn(NH_3)_3OH]^+$ resulted in only one EC **1**. Analogously to the CO_2 pathway, the EC **1** is slightly higher in energy than the separated educts. The geometry of the catalyst in the EC differs from that of the free Model **I**. Due to the interaction of the lone pair of the hydroxide ion with one hydrogen of the **ITCN** methyl group, the previously mentioned distortion of the tetrahedral geometry is widely removed.

A further difference to the CO_2 case results from the asymmetrically cumulated bond system of **ITCN**. Due to the known affinity of sulfur to zinc the transition state of the rate-determining step with a sulfur-coordinated **ITCN** is expected to be less energetic. Scheme 4 shows the three relevant transition structures. The nucleophilic attack of the nitrogen on zinc via **N2(ts)** is not the preferred one. With a difference of around 15 kJ/mol it is significantly higher in energy than transition state **2a(ts)**. The difference between **2a(ts)** and **2b(ts)** is small. As it is just slightly over the limit of accuracy for our computational method, it is too small to substantiate an explicit preference of one of these transition states.

All three transition states form pentacoordinated structures. The geometries of **2a(ts)** and **N2(ts)** are almost ideal trigonal bipyramides where the hydroxide ion and two ammonia ligands occupy the equatorial and the sulfur or nitrogen atom of **ITCN** and the third ammonia ligand the axial positions. Comparatively, **2b(ts)** represents an early transition structure where the former catalyst has almost the same geometry as in **1**.

Both transition structures **2a(ts)** and **2b(ts)** are converted into an intermediate where the zinc atom coordinates to the sulfur of the former **ITCN** (for more details cf. Scheme 4). The intermediates do not only differ in their Gibbs free energies but also in their possible formation mechanisms. Although there is a slight preference of **2a(ts)** compared to **2b(ts)**, it cannot be excluded that the most stable intermediate **3b** is formed not via **2b(ts)** but via **3a** and the corresponding transition structure **3a23b(ts)** which connects these structures by an inversion of the Me-N moiety. Though **3b** is almost 30 kJ/mol more stable than **3a** it seems more reasonable to prefer the pathway via **2b(ts)**.

In continuation and analogously to the pathway of CO_2 (Scheme 1) for **3a** or **3b**, the Lindskog [52] and/or Lipscomb [53] reaction paths have to be taken into account (Scheme 4 and Fig. 3). Although these mechanisms presumably do not exist in the enzymatic reaction path, they are the only possible mechanisms for model catalysts without any polypeptide backbone. As a result of the position of the methyl group, intermediate **3a** can only react via a Lindskog mechanism (i.e., a rotation around the S-C bond by 180°), whereas intermediate **3b** utilizes a Lipscomb transition state **5sh(ts)** where the proton is shifted to the nitrogen.

When a water molecule approaches **3b**, **4sh** will be formed without any barrier (Scheme 4). This intermediate can react via a proton-shuttled transition structure **5sh(ts)** to give **6sh**. Then water leaves **6sh** to form **7sh_A** which is again a barrier-free mechanism. Presumably as a result of the convenient properties of the six ring transition structure **5sh (ts)**, the proton-shift is highly preferred compared to the rotation mechanism. The rotation mechanism requires a high activation Gibbs free energy due to steric interference and hydrogen bridging bonding. These results indicate that the most plausible mechanism is that one which proceeds via the proton-shift (**5sh(ts)**). Another reason is the high thermodynamic preference by the huge difference in free enthalpies of **7rot_A** and **7sh_A**, if both pathways are in equilibrium.

As expected, the structure with the carbonyl moiety (**7sh_A**, −101 kJ/mol relative to the separated reactants, and **7sh_B**, −102 kJ/mol) are the preferred intermediates compared with **7rot_A**, **3a**, and **3b**. This obviously results from the better stabilized C=O double bond and the pronounced delocalization of the nitrogen lone pair into the π system. A NBO calculation of **7sh_A** confirms the p-orbital characteristics of the nitrogen lone pair as well as the

Scheme 4 The mechanism of the **ITCN** pathway-part I. Gibbs free energies in kJ/mol are relative to the separated reactants

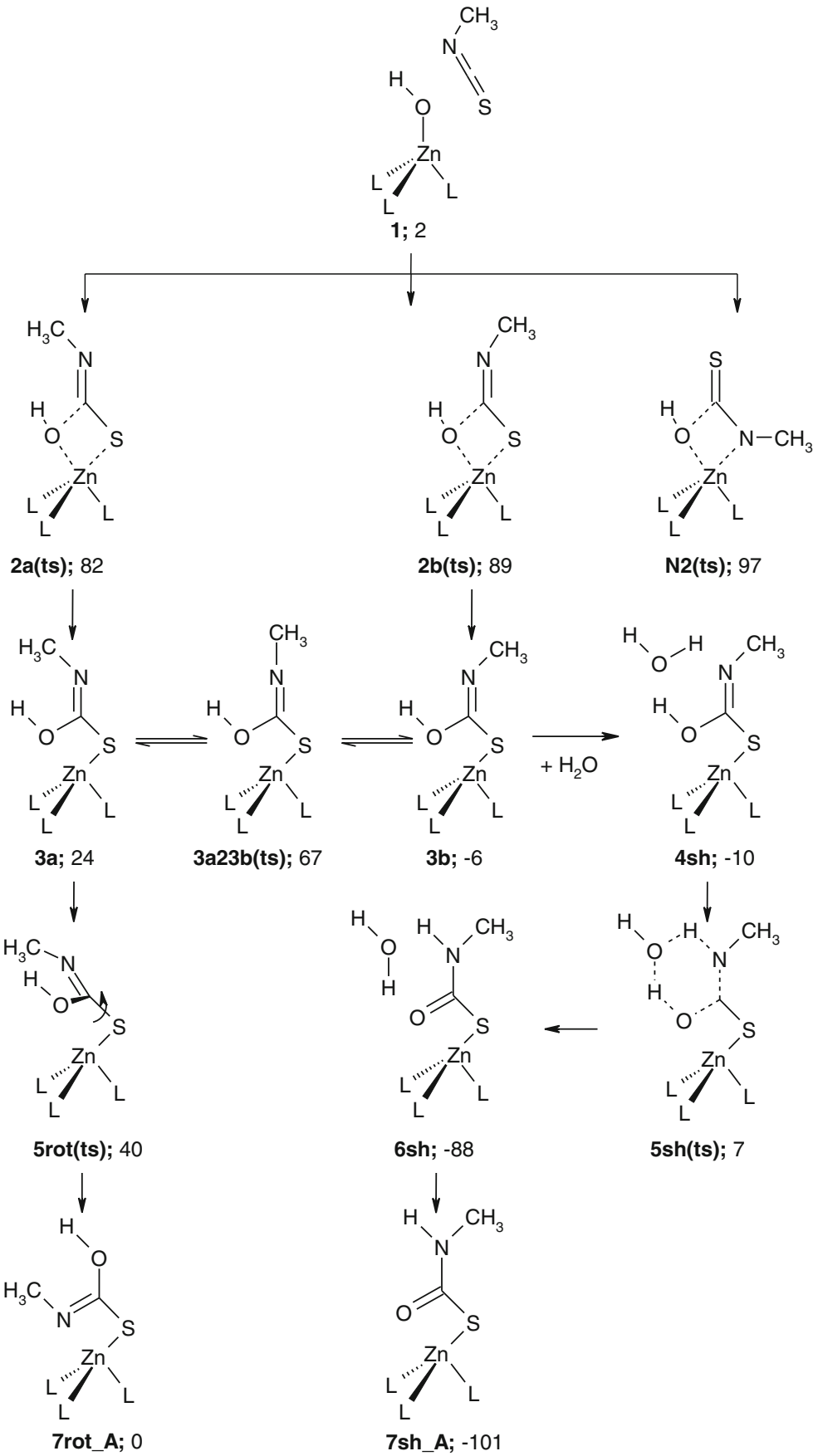

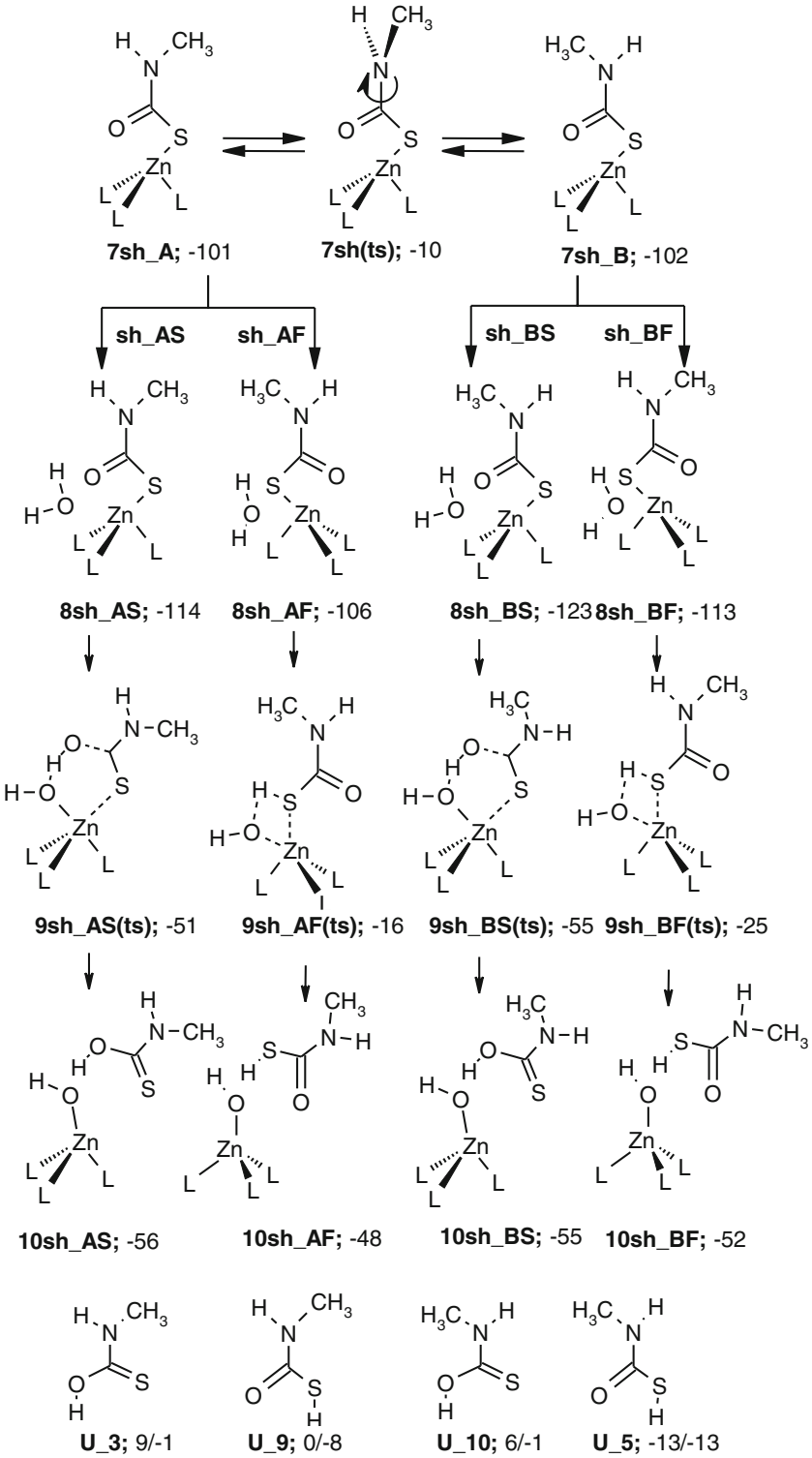

Scheme 5 The mechanism of the **ITCN** pathway-part II. Gibbs free energies in kJ/mol are relative to the separated reactants

strong delocalization into the C=O double bond system. Therefore no elongation of the C-S or the C-N bond due to negative hyperconjugational effects is observed. Hence the Lipscomb reaction step is not only kinetically but also thermodynamically preferred compared to the Lindskog mechanism. The differences in enthalpy of the other three structures (**7rot_A** (Fig. 3), **3a**, and **3b** (Fig. 2)) result from other effects. As the methyl group bonded to the nitrogen atom stands away from the hydroxyl group in **3b**, it first possesses lower sterical interaction between the hydroxyl

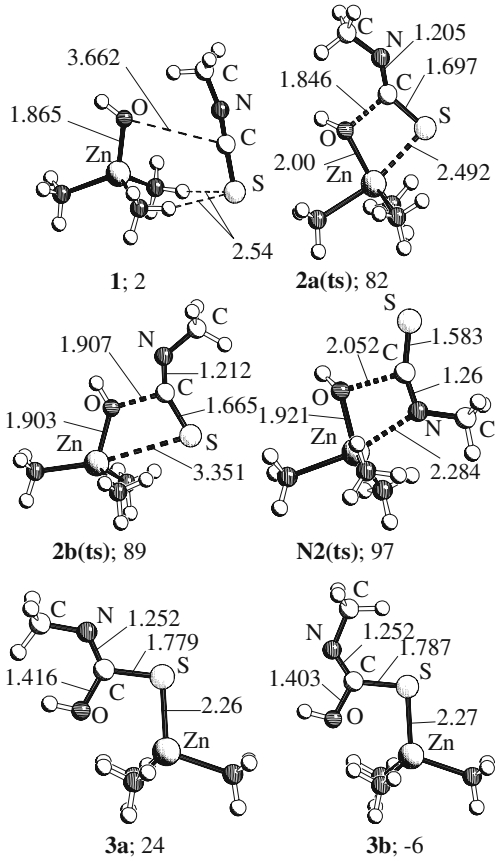

Fig. 2 Essential structures of the **ITCN** hydration pathway

proton and the methyl protons, second there are lone pair repulsion effects between sulfur and nitrogen in structure **3a** and third the lone pair of the nitrogen has a significant negative hyperconjugational effect on the C-S (n_N-$\sigma^*_{(CS)}$) bond and surprisingly on the C-O bond (n_N-$\sigma^*_{(CO)}$), too.

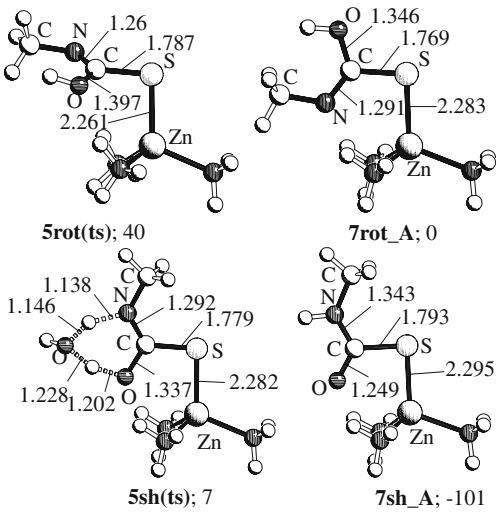

Fig. 3 Lindskog and Lipscomb transition states and intermediates

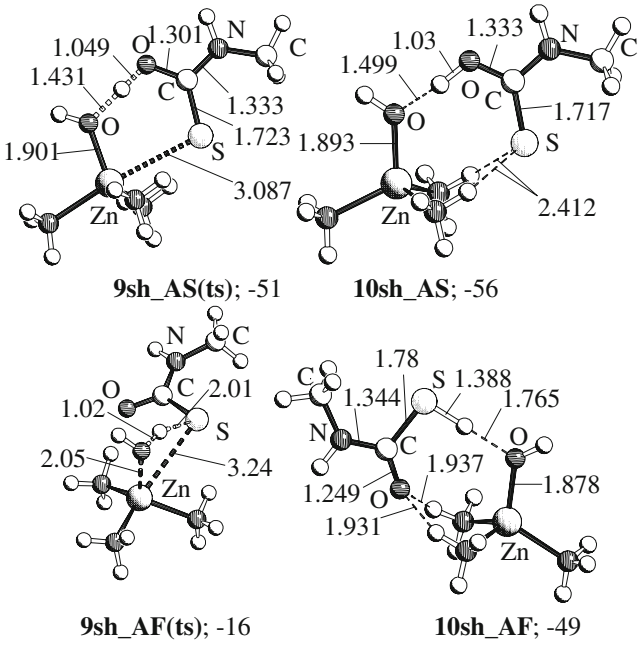

Fig. 4 Two possible water attack transition structures and their corresponding intermediates

This was verified by a NBO calculation, where **7rot_A** and **3a** have only a significant negative hyperconjugational effect on the C-O bond (n_N-$\sigma^*_{(CO)}$). However, they differ in the alignment of the NCO moiety to the Zn-S bond and the rotation angle of the methyl group. As the methyl group and the N-C bond are staggered in **7rot_A**, they have less sterical interaction than in **3a**. There exists no minimum in **3a** for structures in which the methyl group has a staggered conformation. Another reason for the lower enthalpy of **7rot_A** are hydrogen bridge interactions between the lone pair of either the nitrogen in the case of **7rot_A** or the oxygen (**3a**) atom and the σ*-orbital of the H-N bond in the ammonia ligands. NBO calculations show an enthalpy decrease of about 14 kJ/mol in the case of **7rot_A**.

We also calculated the full reaction scope following the **N2(ts)** transition state. Though there are some exothermic reaction paths, they are kinetically unfavored. Both Lindskog and Lipscomb transition states possess higher activation energies than in the case of **5sh(ts)** and **5rot(ts)** (Fig. 3). Details for these reaction mechanisms can be found in the Supporting Information.

The next logical step must be the nucleophilic attack of water (Scheme 5). Analogously to the CO_2 pathway, the oxygen of the water molecule will attack the zinc atom to regenerate the catalytic (model) complex. Again we calculated the full reaction path starting with **7rot_A**, **7rot_B**, **7sh_A** and **7sh_B** taking the possibility of the rotation of the OH (**7rot(ts)**) or $HNCH_3$-moiety (**7sh(ts)**) into account. Here we will concentrate on the mechanisms starting with **7sh_A** and **7sh_B**, as only they are kinetically

and thermodynamically favored. Further mechanistic aspects can be found in the Supporting Information.

No transition state was found when the water molecule approaches the sphere of **7sh_A** and **7sh_B**. Due to the asymmetrically cumulated bond system of **ITCN** a proton from the external water molecule could be shifted either to the sulfur or to the oxygen of the former **ITCN** (**8sh_AS**, **8sh_AF**, **8sh_BS** and **8sh_BF** in Scheme 5).

8sh_AS and **8sh_AF** represent the two possible ECs between **7sh_A** and water, which both possess very low Gibbs free energies relative to the separated reactants. From these two EC's two pathways, which lead to different products, are possible. Structure **9sh_AS(ts)**, where the proton is shifted to the oxygen, is a very late transition state since the proton-shift has already occurred. The negative frequency is related to the dissociation of the S-Zn bond, which is expected to be delayed because of the great affinity of sulfur to zinc. The activation enthalpy of **9a_AS (ts)** is approximately 63 kJ/mol, whereas the resulting EC **10sh_AS** of Model **I** and carbamatic acid is about 59 kJ/mol higher in energy than **8sh_AS**. Furthermore, no intermediate was found where water coordinates to the zinc atom before or after the transition step **9sh_AS(ts)**. This represents another difference to the CO_2 pathway (**CO_2_6**). [54]

Alternatively the proton can be shifted to the sulfur atom. This transition structure **9sh_AF(ts)** behaves like **CO_2_7(ts)** in the CO_2 pathway. Here the hydrogen is shifted to the sulfur (activation barrier 90 kJ/mol). As the pathway following **8sh_AS** is kinetically and the other one thermodynamically favored, we can not predict, which pathway is more probable. This mainly depends on the chosen reaction conditions.

Analogously to the pathway over **7sh_A**, **7sh_B** allows two other mechanisms (Scheme 5). As the activation barrier of **7sh(ts)** is 90 kJ/mol, it seems to be surmountable, but in comparison with the pathways following **7sh_A** it is less probable. The reaction paths are similar to the mechanism described above.

Both pathways give carbamatic or carbamatic-S-acid. As the exothermic and kinetical differences are too small, the calculation can not predict a certain pathway. This seems to depend on the kind of isothiocyanate and the reaction conditions.

Comparison of the substrates ITCN and CO_2

The structural properties of the ECs of both pathways (**ITCN** and CO_2) are quite similar but differ significantly in their Gibbs free energies. Both **ITCN** and CO_2 form endothermic ECs (Fig. 5). The reaction with **ITCN** differs in the type of rate-determining step because of the asymmetrical cumulated bond system of the substrate. **ITCN** prefers the electrophilic zinc-sulfur attack. As CO_2 possesses a higher symmetry than **ITCN**, it forms only one

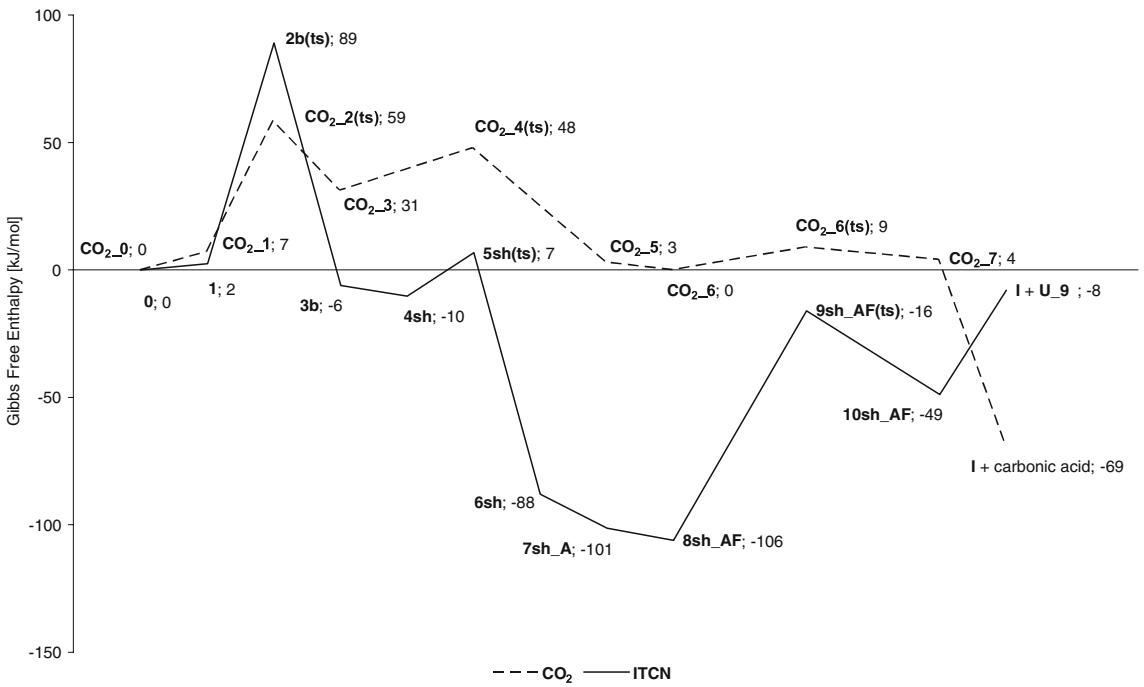

Fig. 5 Gibbs free energies of the two most favorable pathways of **ITCN** (**sh-AF** and **sh-AS**) and CO_2

possible transition state. If we compare the Gibbs free energies of the catalyzed and uncatalyzed reactions of CO_2 and **ITCN**, a significant difference can be seen (cf. Fig. 5 and Table 2). While Model **I** lowers the Gibbs free energy of the rate determining **CO_2_2(ts)** step in the CO_2 pathway by about 25 kJ/mol, the Gibbs free energy is decreased by about 80 kJ/mol in the **ITCN** pathway.

Further, **ITCN** prefers definitely the pathway via the water catalyzed proton-shift (Lipscomb transition state), whereas the situation in the CO_2 pathway is ambiguous [14]. The **ITCN** catalytic cycle differs further as the two intermediates following the rate-determining step permit either a Lindskog- or a Lipscomb-like transition state. While the pathways are sufficiently similar in enthalpy at the point of the Lindskog- or Lipscomb-like transition states, they differ vastly in their resulting intermediates. The CO_2 pathway proceeds about 0 kJ/mol relative to its educts, whereas **ITCN** (**8sh_AF**, Scheme 5; −106 kJ/mol) forms a very stable intermediate. This could become problematic for a realistic catalytic cycle since it will require more energy to surmount the subsequent transition states such as **9sh_AF(ts)** (Scheme 5 and Fig. 4).

The asymmetrically cumulated bond system of **ITCN** also influences the water-attack transition states such as **9sh_AF(ts)** (Scheme 5). While in the CO_2 pathway only one possible transition state exists, the water molecule is able to shift its proton to either the nitrogen or sulfur atoms in the case of **ITCN**. The rate-determining transition state in the CO_2 pathway is energetically very low and therefore forms a very flat hyper surface [47, 54]. This is supported by the small energetic difference to the consecutive intermediate of carbonic acid and Model **I**. While **ITCN** behaves similarly at this point, the energetic difference of the transition state to the preceding intermediate is very large (63 kJ/mol, difference between **9sh_AF(ts)** and **8sh_AF**, Scheme 5). At this point the pathway does not form a "flat" hypersurface. Unfortunately, the pathway of **ITCN** provides a well-stabilized minimum (**8sh_AF**), which could behave as an energetic trap and disable the catalytic cycle.

Finally, both pathways are exothermic. The strongest thermodynamic preference is seen in the case of CO_2, where the carbonic anhydrase product is −69 kJ/mol more stable than the free reactants.

Table 2 Gibbs free energies of the rate-determining steps in all catalytic cycles in [kJ/mol]

	CO_2	ITCN
Catalyzed	59	89
Uncatalyzed	74	158

Comparison of several ITCN substrates

To investigate the influence of the **ITCN** substituent on the Gibbs free energies of the three possible transition states such as **2a(ts)**, **2b(ts)** and **N2(ts)**, we calculated all structures up to the first intermediates (**3a**, **3b** and **N3**) with several substrate examples. To simulate inductive effects, we used methyl-, ethyl- and trifluormethylisothiocyanate (**Me**, **Et**, **CF_3**). These compounds are suitable to simulate the sterical and electronic influence of both the length of an aliphatic residue and the substitution with residues with a high electronegativity. Resonance effects are incorporated by examples such as phenyl-, p-nitrophenyl- and 2,4-dinitrophenylisothiocyanate (**Ph**, **nPh**, **dnPh**). The nitrophenyl residues represent structures with aromatic ring systems of low electron density.

In most cases intermediates comparable with **3b** (Scheme 4) are thermodynamically preferred. **2a(ts)** is the energetically lowest transition state followed by **2b(ts)** and **N2(ts)**. In the case of trifluoromethylisothiocyanate (**CF_3**) the DFT method is not able to differentiate between **2b(ts)** and **N2(ts)** and the thermodynamically lowest intermediate is not **3b** but **N3** (cf. Supporting Information).

The influence of the residue seems to be dominated primarily by inductive effects, since the residue with the strongest electron withdrawing effect is trifluoromethyl. The electron density which is pulled away by the residue is equalized by the electronegativity of nitrogen, which is higher than the electronegativity of sulfur and carbon. As a result, an electron withdrawing group decreases the electron density from the cumulated bond system and predominantly from sulfur. Therefore, at least the sulfur atom of isothiocyanates carrying a strong electron withdrawing residue possesses a low electron density whereas the influence of resonance effects on the cumulated bond system is significantly lower. This can be verified by a NPA analysis as shown in Table 3.

Isothiocyanates with electron withdrawing residues tend to have energetically lower transition states in which the nitrogen atom forms a bond to the zinc ion, as can be seen in the transition states of trifluoromethylisothiocyanate (cf. Table 4). All other residues are not able to pull such a high electron density away from the molecule. Even the aromatic residues do not have a significant influence, which

Table 3 Charges on the atoms of the different isothiocyanates C_{res}-N=C=S

Atom	Me	Et	CF_3	Ph	nPh	dnPh
C_{res}	−0.36	−0.18	1.18	0.12	0.15	0.14
N	−0.44	−0.44	−0.54	−0.44	−0.45	−0.46
C	0.23	0.22	0.23	0.23	0.23	0.22
S	−0.04	−0.04	0.23	−0.00	0.05	0.09

Table 4 Residue-depending free enthalpies of the rate determining steps

	Me	Et	CF_3	Ph	nPh	dnPh
2a(ts)	82	77	89	79	93	97
2b(ts)	89	88	90	92	102	103
N2(ts)	97	101	74	102	109	126

presumably is related to their bulky character and the resulting steric repulsion.

Solvent corrections

To examine the influence of a solvent, all three possible rate-determining steps in the **ITCN** pathway (**2a(ts)**, **2b(ts)** and **N2(ts)**), EC **1** and the first intermediates beyond the transition states (**3a**, **3b**, **N3**) were calculated using the C-PCM model and several solvents (heptane, chloroform, dichloroethane, acetonitrile, and water). All solvent calculations include full geometry optimizations starting with the gas-phase structure.

With all solvent variations the Gibbs free energy of the rate-determining steps rises in comparison to the gas phase. A rise of about 30 kJ/mol was observed. There is no linear correlation between the applied solvent and the increase in Gibbs free energy of the first transition state. The Gibbs free energy of the intermediates mostly increases by about 10 kJ/mol except for **N3**.

The solvent also has an effect on the selectivity of the reaction. All three transition structures possess similar Gibbs free energies, wherefore no kinetic selectivity can be predicted. Since the intermediate **N3** is strongly favored compared to **3a** and **3b** (20–25 kJ/mol), the **ITCN** catalytic cycle prefers in solution the addition to the C=N double bond. In summary, the solvent has a significant influence on the selectivity of the reactions as it changes the rate-determining step in both pathways. The catalytic effect, however, does not vanish since in all cases a decrease of about 70 kJ/mol compared with the uncatalyzed reaction can be found.

Further catalytic models

As our goal is the introduction of enzyme strategies to synthetic chemistry, we calculated the free enthalpies of the pathway with catalytic models, which are used in our laboratory. Well known models for HCAII are zinc-hydroxide complexes with [12]aneN_3 and [12]aneN_4-Ligands [55, 56].

The free enthalpies listed in Table 5 demonstrate that Model **I** is suitable to describe the essential structures and energetic properties correctly and comparably to the results from models like [12]aneN_3 and [12]aneN_4. Especially the similarity between the free enthalpies of Model **I** and [12]aneN_4 is outstanding.

Table 5 Free enthalpies for different models

	NH_3	[12]aneN_3	[12]aneN_4
0	0	0	0
1	2	12	8
2b(ts)	89	103	92
3b	−6	−3	−10
4sh	−10	−9	−14
5sh(ts)	7	20	5
6sh	−88	−82	−87
7sh_A	−101	−90	−100

Conclusions

From the investigation reported herein we conclude, that a zinc-complex such as Model **I** and related structures are able to significantly decrease the Gibbs free energy of the rate-determining step of the title reaction. Even though the mechanism to some extent follows the catalytic cycle of CO_2 predetermined by nature, there are many differences in enthalpies and structures.

As the substrate possesses an asymmetrically cumulated bond system, it allows multiple structural variants for the rate-determining steps. Unfortunately, the energetic differences between these transition states are too low to give an explicit answer to the question of kinetic control. However, intermediates with very low Gibbs free energies exist (**7sh_A** and **7sh_B**), thus a thermodynamical control is given.

Although the Gibbs free energy of the rate-determining step is slightly higher than in the natural catalytic cycle with CO_2, the catalytic effect in comparison to the uncatalyzed reaction is remarkably expressed. The Lipscomb transition structure characterizes the preferred pathway, whereas the CO_2 pathway shows no definite preference.

As a result from the asymmetrically cumulated bond system the hydration step could be performed via two different transition structures. The responsible transition structures leads to different products, which differ vastly in their Gibbs free energy. Therefore, the hydration step is dominated by a thermodynamical control.

Solvent corrections in the calculation lead to a slightly higher rate-determining step and a lower selectivity as the three possible rate-determining steps possess nearly the same Gibbs free energy. Yet, the catalytic effect is still present in solution.

One way to control the selectivity might be the variation of the cumulene residue; R. Strong electron-withdrawing

residues generate the largest effect, inductive effects are more important than resonance effects.

Some of the results presented herein should be transferable to stoichiometric syntheses with an appropriate catalytic model such as the [12]aneN$_3$ or [12]aneN$_4$ zinc hydroxide complexes[48, 57–59]. We are currently working on further experimental and computational investigations with the appropriate model chosen for this reaction. Comparing with the CO_2 substrate, the mechanisms we investigated indicate a higher activation energy for the rate determining step in the case of **ITCN** and, as recently published, of the COS case. This obviously is one reason why nature developed a procedure via CO_2 as the preferred cumulenic substrate. Nevertheless, it should be possible to close the gap between the native CAs and the synthetic reality as in all cases the zinc-complex mediated catalysis is expressed to significant extent.

Acknowledgments Financial support by the Deutsche Forschungsgemeinschaft (Collaborative Research Center 436, University of Jena, Germany), the Fonds der Chemischen Industrie (Germany), and the Thüringer Ministerium für Wissenschaft, Forschung und Kunst (Erfurt, Germany) is gratefully acknowledged.

References

1. Thoms S (2002) J Theor Biol 215:399–404. doi:10.1006/jtbi.2002.2528
2. Bertini I, Luchinat C (1983) Acc Chem Res 16:272–279. doi:10.1021/ar00092a002
3. Silverman DN, Lindskog S (1988) Acc Chem Res 21:30–36. doi:10.1021/ar00145a005
4. Christianson DW, Fierke CA (1996) Acc Chem Res 29:331–339. doi:10.1021/ar9501232
5. Lipscomb WN, Norbert S (1996) Chem Rev 96:2375–2433. doi:10.1021/cr950042j
6. Maren TH (1967) Physiol Rev 47:595–781
7. Tashian RE (1989) Bioessays 10:186–192. doi:10.1002/bies.950100603
8. Khalifah RG (1971) J Biol Chem 246:2561–2573
9. Heck RW, Boriack-Sjodin AP, Qian M, Tu C, Christianson WD, Laipis JP, Silverman ND (1996) Biochemistry 35:11605–11611. doi:10.1021/bi9608018
10. Hartmann M, Clark T, van Eldik R (1996) J Mol Model 2:358–361. doi:10.1007/s0089460020358
11. Hartmann M, Merz JKM, van Eldik R, Clark T (1998) J Mol Model 4:355–365. doi:10.1007/s008940050094
12. Merz JKM, Hoffmann R, Dewar MJS (1989) J Am Chem Soc 111:5636–5649. doi:10.1021/ja00197a021
13. Muguruma C (1999) THEOCHEM 461–462:439–452. doi:10.1016/S0166-1280(98)00455-2
14. Schenk S, Kesselmeier J, Anders E (2004) Chem Eur J 10:3091–3105. doi:10.1002/chem.200305754
15. Notni J, Schenk S, Protschill-Krebs G, Kesselmeier J, Anders E (2007) ChemBioChem 8:530–536. doi:10.1002/cbic.200600436
16. Notni J, Schenk S, Görls H, Breitzke H, Anders E (2008) Inorg Chem 47:1382–1390. doi:10.1021/ic701899u
17. Mauksch M, Bräuer M, Weston J, Anders E (2001) ChemBioChem 2:190–198. doi:10.1002/1439-7633(20010302)2:3<190::AID-CBIC190>3.0.CO;2-7
18. Schröder D, Schwarz H, Schenk S, Anders E (2003) Angew Chem Int Ed 42:5087–5090. doi:10.1002/anie.200351440
19. Prince RH, Woolley PR (1973) Bioorg Chem 2:337–344. doi:10.1016/0045-2068(73)90034-5
20. Tautermann CS, Loferer MJ, Voegele AF, Liedl KR (2003) J Phys Chem B 107:12013–12020. doi:10.1021/jp0353789
21. Sola M, Lledos A, Duran M, Bertran J (1992) J Am Chem Soc 114:869–877. doi:10.1021/ja00029a010
22. Pocker Y, Deits TL (1982) J Am Chem Soc 104:2424–2434. doi:10.1021/ja00373a016
23. Nakata K, Shimomura N, Shiina N, Izumi M, Ichikawa K, Shiro M (2002) J Inorg Biochem 89:255–266. doi:10.1016/S0162-0134(01)00419-6
24. Lee C, Yang W, Parr RG (1988) Phys Rev B Condens Matter Mater Phys 37:785–789
25. Becke AD (1993) J Chem Phys 98:5648–5652. doi:10.1063/1.464913
26. McLean AD, Chandler GS (1980) J Chem Phys 72:5639–5648. doi:10.1063/1.438980
27. Krishnan R, Binkley JS, Seeger R, Pople JA (1980) J Chem Phys 72:650–654. doi:10.1063/1.438955
28. Frisch MJ, Head-Gordon M, Pople JA (1990) Chem Phys Lett 166:275–280. doi:10.1016/0009-2614(90)80029-D
29. Head-Gordon M, Pople JA, Frisch MJ (1988) Chem Phys Lett 153:503–506. doi:10.1016/0009-2614(88)85250-3
30. David EW, Dunning TH Jr (1993) J Chem Phys 98:1358–1371. doi:10.1063/1.464634
31. Rick AK, Dunning TH Jr, Robert JH (1992) J Chem Phys 96:6796–6806. doi:10.1063/1.462569
32. Barone V, Cossi M (1998) J Phys Chem A 102:1995–2001. doi:10.1021/jp9716997
33. Cossi M, Rega N, Scalmani G, Barone V (2003) J Comput Chem 24:669–681. doi:10.1002/jcc.10189
34. Klamt A, Schüürmann G (1993) J Chem Soc Perkin Trans 2:799–805. doi:10.1039/p29930000799
35. Frisch MJ, Trucks GW, Schlegel HB, Scuseria GE, Robb MA, Cheeseman JR, Montgomery JA Jr, Vreven T, Kudin KN, Burant JC, Millam JM, Iyengar SS, Tomasi J, Barone V, Mennucci B, Cossi M, Scalmani G, Rega N, Petersson GA, Nakatsuji H, Hada M, Ehara M, Toyota K, Fukuda R, Hasegawa J, Ishida M, Nakajima T, Honda Y, Kitao O, Nakai H, Klene M, Li X, Knox JE, Hratchian HP, Cross JB, Adamo C, Jaramillo J, Gomperts R, Stratmann RE, Yazyev O, Austin AJ, Cammi R, Pomelli C, Ochterski JW, Ayala PY, Morokuma K, Voth GA, Salvador P, Dannenberg JJ, Zakrzewski VG, Dapprich S, Daniels AD, Strain MC, Farkas O, Malick DK, Rabuck AD, Raghavachari K, Foresman JB, Ortiz JV, Cui Q, Baboul AG, Clifford S, Cioslowski J, Stefanov BB, Liu G, Liashenko A, Piskorz P, Komaromi I, Martin RL, Fox DJ, Keith T, Al-Laham MA, Peng CY, Nanayakkara A, Challacombe M, Gill PMW, Johnson B, Chen W, Wong MW, Gonzalez C, Pople JA (2004) Gaussian03 revision D.01. Gaussian, Inc., Wallingford, CT
36. Glendening ED, Badenhoop JK, Reed AE, Carpenter JE, Bohmann JA, Morales CM, Weinhold F (2001) NBO 5.0 Theroretical Chemistry Institute, University of Winsconsin, Madison
37. Reed AE, Curtiss LA, Weinhold F (1988) Chem Rev 88:899–926. doi:10.1021/cr00088a005
38. Reed AE, Weinstock RB, Weinhold F (1985) J Chem Phys 83:735–746. doi:10.1063/1.449486
39. Reed AE, Weinhold F (1983) J Chem Phys 78:4066–4073. doi:10.1063/1.445134
40. Hagemann H (1983) Methoden d.r Organischen Chemie (Houben-Weyl): Kohlensaeure-Derivate. Georg Thieme Verlag, Stuttgart

41. Walter W, Bode KD (1967) Angew 7:285–328. doi:10.1002/ange.19670790702
42. Browne DW, Dyson GM (1931) J Chem Soc 3285–3308. doi:10.1039/jr9310003285
43. Rao CNR, Venkataraghavan R (1962) Tetrahedron 18:531–537. doi:10.1016/S0040-4020(01)92703-6
44. Harris JF (1960) J Am Chem Soc 82:155–158. doi:10.1021/ja01486a036
45. Hadad CM, Rablen PR, Wiberg KB (1998) J Org Chem 63:8668–8681. doi:10.1021/jo972180+
46. Nilsson Lill SO, Rauhut G, Anders E (2003) Chem Eur J 9:3143–3153. doi:10.1002/chem.200304878
47. Bottoni A, Lanza CZ, Miscione GP, Spinelli D (2004) J Am Chem Soc 126:1542–1550. doi:10.1021/ja030336j
48. Kimura E (2001) Acc Chem Res 34:171–179. doi:10.1021/ar000001w
49. Mulliken RS (1955) J Chem Phys 23:1833–1840. doi:10.1063/1.1740588
50. Fonseca Guerra C, Handgraaf J-W, Baerends EJ, Bickelhaupt FM (2004) J Comput Chem 25:189–210. doi:10.1002/jcc.10351
51. Eriksson AE, Jones TA, Liljas A (1988) Prot Struct Funct Genet 4:274–282. doi:10.1002/prot.340040406
52. Lindskog S, Engberg P, Forsman C, Ibrahim AS, Jonsson HB, Simonsson I, Tibell L (1987) Ann N Y Acad Sci 429:61–75. doi:10.1111/j.1749-6632.1984.tb12315.x
53. Liang J-Y, Lipscomb WN (1987) Biochemistry 26:5293–5301. doi:10.1021/bi00391a012
54. Miscione GP, Stenta M, Spinelli D, Anders E, Bottoni A (2007) Theor Chem Acc 118:193–201. doi:10.1007/s00214-007-0274-x
55. Notni J, Günther W, Anders E (2007) Eur J Inorg Chem 7:985–993. doi:10.1002/ejic.200600962
56. Notni J, Schenk S, Roth A, Plass W, Görls H, Uhlemann U, Walter A, Schmitt M, Popp J, Chatzipapadopoulos S, Emmler T, Breitzke H, Leppert J, Buntkowsky G, Kempe K, Anders E (2006) Eur J Inorg Chem 14:2783–2791. doi:10.1002/ejic.200500948
57. Kimura E (1994) Prog Inorg Chem 41:443–491. doi:10.1002/9780470166420.ch6
58. Kimura E, Koike T, Shionoya M (1997) Struct Bond 89:1–28
59. Kimura E, Shiota T, Koike T, Shiro M, Kodama M (1990) J Am Chem Soc 112:5805–5811. doi:10.1021/ja00171a020